Check for updates

Depolymerization of PET by common alkanolamines yields tunable monomers to expand the design space of 3D-printable, intrinsically self-healing polyamide-ionenes†

Mousumi R. Bepari, [ID] Pravin S. Shinde [ID] and Jason E. Bara [ID] *

Polyethylene terephthalate (PET), a ubiquitous thermoplastic used in textiles and packaging, is one of the primary contributors to plastic pollution. While PET is also one of the most recycled plastics, it has value as a rich source of chemical building blocks. When PET is depolymerized by amino alcohols ("alkanolamines") such as monoethanolamine (MEA), terephthalamide-diol molecules are produced. In the presence of thionyl chloride (SOCl₂), these diols are amenable to transformation to the corresponding dichloride monomers, which can then be polymerized *via* condensation methods (*i.e.*, Menshutkin reaction) with bisimidazole compounds followed by ion-exchange to yield polyamide (PA)-ionenes with tailored structures. The PA-ionenes produced from these methods are intrinsically self-healing and possess thermal and mechanical properties which make them amenable to 3D printing. This study reports on synthetic methods and structure–property relationships in PA-ionenes that arise from the choice of molecular building blocks.

1. Introduction

The mass production of fossil fuel-derived plastics and the accompanying environmental pollution from plastic waste demands attention to the sustainability of plastic materials. Currently, approximately 380 Mt of plastic waste is generated annually, and the recycling rate is well below the production rate, with 85% of plastics destined for landfills.[1–4] Chemical recycling is possibly the only economically viable approach to suppress the environmental impacts of plastic wastes while extracting value in the form of recovered monomers (*e.g.*, terephthalic acid (TA) and ethylene glycol (EG) from PET) and/or new molecular products. Chemical recycling may be superior to thermomechanical recycling, which will only degrade polymers over time through oxidation, chain scission, and introduction of impurities.[5] Another effective way of recycling postconsumer wastes could be carbonization by which valuable carbonaceous materials or high surface area activated carbon can be recovered, although the high-temperature requirement often limits the practicability the process.[6]

Among the most common thermoplastic materials, PET ranks 4th in terms of annual global plastic production, follow-

ing the polyolefins—polypropylene (PP), polyethylene (PE), and polyvinyl chloride (PVC).[7] The global PET market was valued at $48 B in 2023 and is expected to expand from $53 B in 2024 to USD $110 B by 2032, reflecting a compound annual growth rate of 9.5% over the projection period.[8] Among commodity plastics, PET is the most readily amenable to chemical recycling due to the susceptibility of the ester group to cleave in the presence of many types of reagents. Depolymerization of PET *via* "chemolysis" can be performed *via* glycolysis to bis (2-hydroxyethyl) terephthalate (BHET), *via* methanolysis to dimethyl terephthalate (DMT), and hydrolysis to TA, all of which could be used to obtain fresh PET.[9]

The use of primary (1°) or secondary (2°) amines to depolymerize PET is also highly effective, and reactions will occur even at ambient temperature. However, in the case of simple alkylamines (*e.g.*, *n*-butylamine), the terephthalamide (TAm) products formed are deactivated and will not have the same utility as BHET, DMT, or TA. Recently, our group has reported a unique depolymerization method called "imidazolysis", wherein PET is depolymerized by imidazole to form "1,1′-terephthaloyl bisimidazole" (TBI), which remains reactive and shows excellent activity forming TA (*via* reaction with water), DMT (*via* reaction with MeOH), and TAm products (*via* reaction with amines).[10] An overview of these methods is illustrated in Fig. 1.

A strategy wherein aminolysis of PET can yield active molecules is to use amino alcohols ("alkanolamines") such as

Department of Chemical & Biological Engineering, The University of Alabama, Tuscaloosa, AL 35487-0203, USA. E-mail: jbara@eng.ua.edu
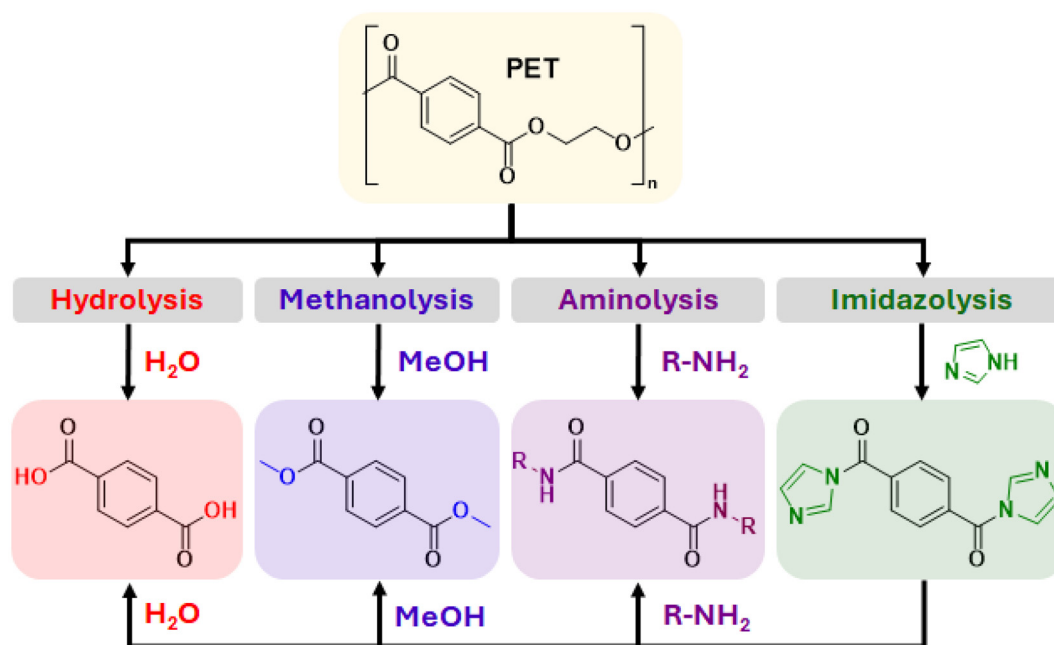
Fig. 1 Common depolymerization methods for PET along with "imidazolysis" (recently reported by our group).

mononethanolamine (MEA). MEA and other alkanolamines are widely used for the removal of CO_2 in carbon capture and gas treating applications.[11,12] Depolymerization of PET by 1° or 2° alkanolamines is expected to proceed *via* reaction with the amine rather than the alcohol, yielding TAm-diol products. TAm-diols generated through these methods have been successfully utilized in preparing resin components for the production of photopolymerizable films and synthesis of low molecular weight poly(ester-amides).[13,14] Given the diversity of alkanolamines that are available (some alkanolamines like MEA are available at very low cost), the depolymerization of PET in this manner presents some unique opportunities for molecular and polymer design, particularly relating to expanding the structural tailoring of polyamide (PA)-ionenes, a class of intrinsically self-healing polymers (ISHPs), on which our group has worked for a number of years.[15]

Ionenes are a category of charged macromolecules distinguished from ionomers and polyelectrolytes as they incorporate an ionic group (usually a cation) directly within their main chain, accompanied by a "free" counterion (usually an anion). The structural diversity of ionenes can be extensively tailored by manipulating the architecture of the ionic groups, choice of spacers and counterions, charge density, and spatial arrangement relative to the potentially functional backbone. The majority of ionenes are synthesized through a Menshutkin polymerization, a process in which two types of bifunctional monomers (typically of the A–A and B–B type) are covalently linked by polycondensation reactions, with the cation and anion formed as a consequence of the reaction. A comprehensive understanding detailing a vast library of ionenes can be found in the recent reviews by O'Harra and Bara.[16,17] To date, our group has developed a variety of ionenes with different

functional groups that are associated with "high-performance" (HP) polymers (*e.g.*, amide, amide–imide, ether–ether–ketone, *etc.*) linked by bisimidazolium units.[18,19] Given the efficacy of ionenes as antimicrobial agents, Tan *et al.* developed hydrophilic ionenes from tertiary (3°) diamines obtained *via* aminolysis of PET and subsequent reaction of the obtained TAm-diamines with α,α′-dichloro-*p*-xylene (pDCXy).[20]
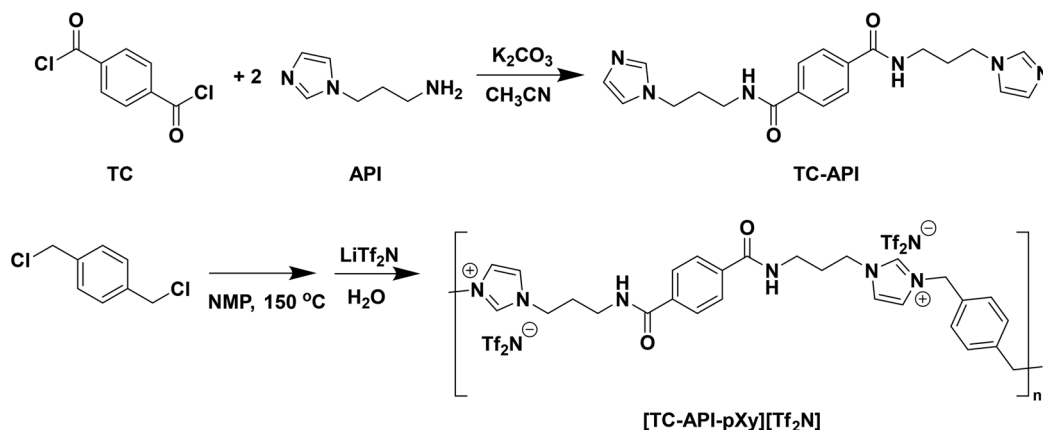
In our prior works studying PA-ionenes, we have relied on the use of 1-(3-aminopropyl) imidazole (API) with terephthaloyl chloride (TC) to produce the "TC-API" bisimidazole TAm molecules which have been the essential building blocks of our PA-ionenes (Scheme 1a). Our group has also collaborated with Demarteau and Sardon to show that TC-API could be produced directly from API and waste PET using their TBD : MSA catalyst.[21] Although effective, these methods are constrained by some limitations on the ability to select/tailor the various components of the monomer units.

API can be produced at industrial scales *via* the reaction of imidazole and acrylonitrile, followed by reduction of the nitrile (−CN) using H_2 with RANEY® Nickel catalyst (Scheme 2a). We also reported that these methods can be extended to the use of 2-methylimidazole with acrylonitrile to form 1-(3-aminopropyl)-2-methylimidazole, and used in the synthesis of polyimide (PI)-ionenes.[22] However, it must be noted that hydrogenation of nitriles to 1° amines using RANEY® Nickel presents hazards due to the pyrophoric nature of the catalyst and the use of aqueous NH_4OH as a co-solvent with MeOH, which requires reaction vessels rated to handle pressures and results in the release of significant amounts of ammonia (NH_3) during reaction workup.
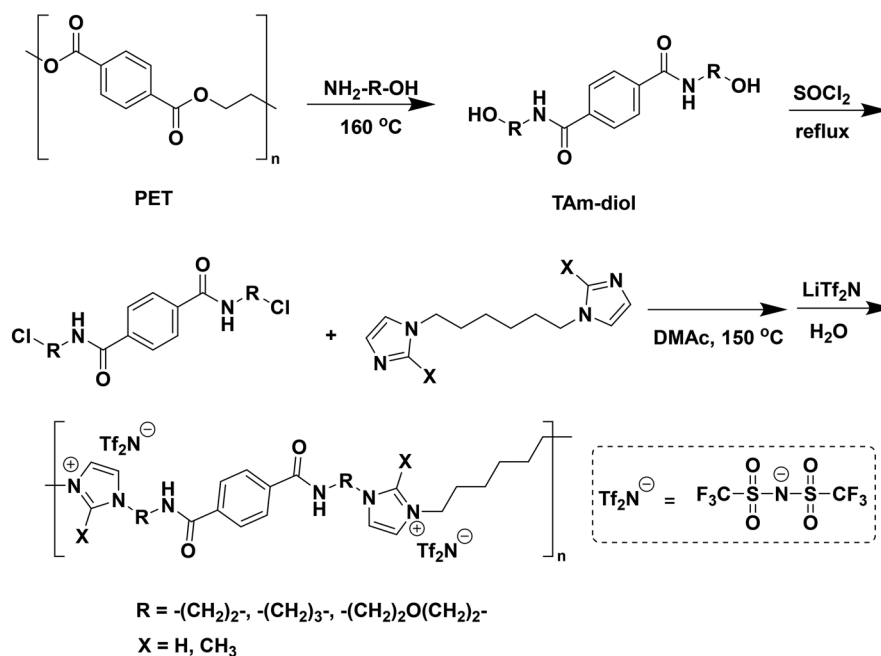
These studies led us to the realization that equivalent PA-ionenes could be constructed *via* a parallel route in which PET

© 2025 The Author(s). Published by the Royal Society of Chemistry

RSC Appl. Polym., 2025, **3**, 686–700 | **687**

Scheme 1 Synthetic routes to PA-ionenes. (a) Prior methods starting from API and dihalide. (b) Methods used in this study, starting from PET and 1° alkanolamines.

is depolymerized *via* 1-amino-3-propanol to form the TAm-diol followed by conversion of –OH groups to –Cl groups with thionyl chloride (SOCl₂), while the requisite bisimidazole monomer could be synthesized from imidazole with pDCXy. The two approaches are illustrated in Scheme 1.

In our prior methods using TC-API (Scheme 1a), the spacer between the TAm and the terminal imidazole rings is fixed at a length of three carbons as API is derived from acrylonitrile (*i.e.*, HC=CH₂–CN). As mentioned, various imidazoles (*e.g.*, 2-methylimidazole, 4-methylimidazole) could be reacted with acrylonitrile to form corresponding 1-(3-aminopropyl)imid-

azole compounds (Scheme 2a) with substituents on C(2), C(4), and/or C(5) positions of the imidazole ring, but this would still not allow for varying the length or chemistry of the linker between the imidazole and 1° amine.

A general method for obtaining imidazoles tethered to a 1° amine *via* the Gabriel Synthesis is shown in Scheme 2b.[23] However, using a Gabriel Synthesis to obtain 1-(2-aminoethyl) imidazole, 1-(4-aminobutyl)imidazole, *etc.*, for the purposes of PA-ionenes might be more labor intensive compared to depolymerizing PET with a corresponding alkanolamine (Scheme 1b) or directly reacting that alkanolamine with TC (Scheme 1a).
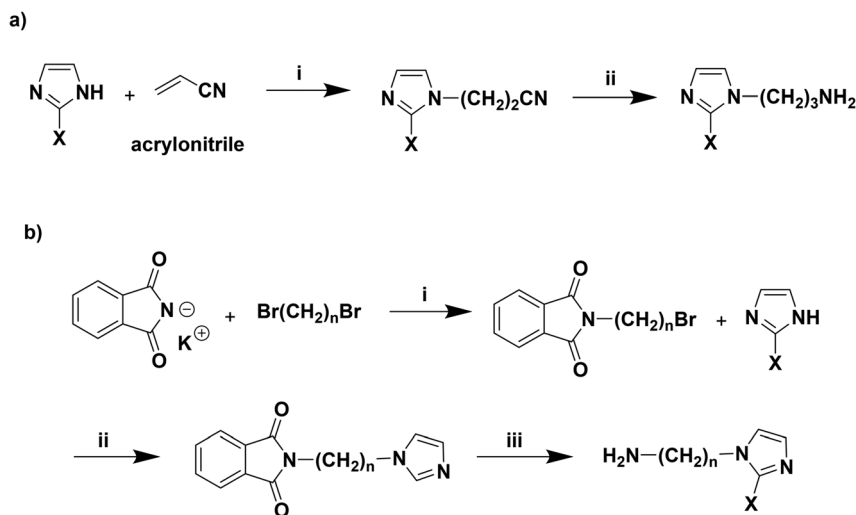
Scheme 2 a) (i) Imidazole and acrylonitrile in presence of Et₃N and toluene produce imidazole-propylnitrile, (ii) reduction to API by H₂ in the presence of RANEY® nickel catalyst in aqueous MeOH/NH₄OH. (b) (i) Phthalimide potassium salt reacting with dibromo-alkane in DMF at 100 °C 24 h to produce N-(ω-Bromoalkyl) phthalimide, (ii) reaction with imidazole compound in DMF at 80 °C for 8 h to produce the imidazole-tethered-phthalimide, (iii) removal of protecting group to obtain corresponding 1-(ω-aminoalkyl) imidazole with hydrazine hydrate in EtOH for 24 h at reflux.

Furthermore, the general method in Scheme 2b could not be directly used to synthesize imidazoles tethered to 2° or 3° amines. Although we did not depolymerize PET by 2° alkanolamines in this study, this will be the subject of future work to understand the impact of H-bonding (*i.e.*, N–H *vs.* N–CH₃) on PA-ionene properties.

Aminolysis of PET by alkanolamines can lead to expanded options for the synthesis of TA ionenes with diverse functional groups with potentially lower costs when using commodity alkanolamines like MEA. Not only can alkanolamines offer different spacer lengths between the imidazole ring and amide group, but the independent synthesis of the bisimidazole monomer leads to options such as the introduction of a methyl group at the C(2) position of the imidazolium ring. As in our prior works, we are interested not only in the thermal and mechanical properties of these self-healing (SH) PA-ionenes but also in their use as feedstocks for fused deposition modeling (FDM) 3D printing, wherein the SH nature of the PA-ionene is expected to minimize or eliminate defects between printed layers.

3D printing (additive manufacturing (AM)) has been a growing area for prototyping and production since the first commercial instruments became available in the late 1980s.[24] FDM (also known as fused filament fabrication (FFF)), is an extrusion-based 3D printing process that works by melting and extruding thermoplastic or elastomeric material to build a product in a layer-by-layer manner using computer-aided design (CAD) files as inputs. However, FDM 3D printing of conventional thermoplastics suffers from issues such as separation of layers, warping, shrinkage while cooling, rough surface finish, environmental sensitivity, poor thermal stability, and the possibility of toxic emissions from polymers like ABS as printing temperatures can exceed 220 °C.[25]

Ionenes may offer some advantages in FDM 3D printing, including low to moderate glass-transition temperatures (T_g), which facilitate printing at lower temperatures and improved thermal stability when anions such as Tf₂N⁻ are present. One current drawback of using ionenes in 3D printing includes a higher cost than commodity polymers like ABS. The intrinsic SH behaviors associated with PA-ionenes also mean that filaments of PA-ionene would inevitably bond to themselves when spooled, thus requiring the use of FDM printers that do not use filaments or some way of "passivating" the filament surface.

Computational analysis of ionic interactions in PA-ionenes has revealed that the intramolecular interactions between electrophilic-nucleophilic ion pairs within each repeating unit, along with H-bonding originating from the TAm moiety and the anion's proximity to the nearest cation, contribute to the SH behaviors and shape recovery characteristics.[26] Therefore, the judicious selection of monomers can endow ionene polymers with strong electrostatic forces and non-covalent H-bonding interactions, improving adhesion and lowering extrusion temperature by overcoming thermal and environmental barriers. The recently developed PA ionene ([TC API pXy][Tf₂N]) (see Scheme 1a) from our group was printed using a 3D Bioplotter. The "dog-bone" sample exhibited an impressive elongation of 445%. Furthermore, the intrinsic SH behaviors were utilized to demonstrate that relatively simplistic 2D objects could be assembled into complex 3D structures that fused together *via* "interfacial welding" (*i.e.*, spontaneous bonding of surfaces without any additional stimuli or reagents).[26]

In earlier research, Long and co-workers developed poly (ether ester) ionomers synthesized from poly(ethylene glycol) (PEG) and sulfonated dimethylisophthalate, which were

© 2025 The Author(s). Published by the Royal Society of Chemistry

RSC Appl. Polym., 2025, **3**, 686–700 | **689**

exchanged with different monovalent and divalent cations. This modification resulted in improved melt viscosity for divalent cations while preserving lower extrusion temperatures.[27] The extended study aimed to investigate the impact of incorporating ionic and non-ionic fillers on 3D printing performance. The findings established that $CaCl_2$ additives interact ionically with the pendant sulfonate groups, reducing warpage and shrinkage upon cooling, outperforming inorganic fillers that only interacted physically and failed to enhance these properties. Additionally, the $CaCl_2$-blended material exhibited the highest modulus and elongation at break.[28] While ionic polymers are beginning to be used in FDM 3D printing, the exploration of ionene materials is still very sparse overall. This research gap leads us to explore the potential of combinations of cation–anion backbone chemistries and their synergistic interactions with charged fillers, specifically ionic liquids (ILs).[24] For instance, adding ILs to ionenes could be a particularly promising method to tune thermal and mechanical properties beyond tailoring the ionene backbone. The solvent (IL)–solute (ionene) interactions can form ionogels, which could improve processability in both conventional extrusion and FDM 3D printing processes.[29]

To advance the aforementioned concepts, we herein present six distinct types of PA-ionene materials synthesized *via* the aminolysis of waste PET by three different 1° alkanolamines. All the ionenes contain two cation–anion pairs in the repeating unit with hexylene spacers between the imidazolium cations. Each PA-ionene was synthesized in two forms of the imidazolium cation: one with $C(2)–H$ and one with $C(2)–CH_3$ to observe the effect of "blocking" this position from interacting with the anion. The structural, mechanical, and thermal properties of the ionenes were thoroughly characterized, and all have utility in FDM 3D printing and experience SH behaviors. This work expands the understanding of structure–property relationships in ionic polymers and potentially opens opportunities for further scale up of PA-ionenes as unique 3D printing feedstocks.

2. Experimental section

2.1 Materials

2-(2-Aminoethoxy)ethanol ("diglycolamine" (DGA), 99%) and sodium hydride (NaH) (60 wt% dispersion in paraffin liquid) were purchased from Tokyo Chemical Industry (TCI) Co., Ltd (Portland, OR, USA). MEA (99%) was purchased from MilliporeSigma (Burlington, MA, USA). Imidazole (99%), pyridine (99%), and activated, basic aluminium oxide (−60 Mesh Powder, S.A. 150 m^2 g^{-1}) were purchased from Beantown Chemical (Hudson, NH, USA). 2-Methylimidazole (97%) was purchased from Alfa Aesar (Ward Hill, MA, USA). 1,6-Dibromohexane (DBH, 98%), triethylamine (Et_3N, 99%), thionyl chloride ($SOCl_2$, 99%), and 3-amino-1-propanol (3A1P, 99%) were purchased from Thermo Scientific (Waltham, MA, USA). 'Lithium bis(trifluoromethylsulfonyl)imide' or 'Lithium bistriflimide' ($LiTf_2N$, supplier name: HQ-115) was purchased

from 3M (Saint Paul, MN, USA). Tetrahydrofuran (THF) (ACS grade) and *N*,*N*-dimethylacetamide (DMAc) (ACS grade) were purchased from VWR. Acetone, dichloromethane (DCM), diethyl ether (Et_2O), ethyl acetate (EtOAc), hexanes (mixture of isomers), chloroform ($CHCl_3$), and methanol (MeOH) were purchased from the stockroom at the University of Alabama (UA) Dept. of Chemistry and Biochemistry at ACS grade or higher. Deionized water ($DI-H_2O$) was obtained from an 18 MW source in the UA Department of Chemistry & Biochemistry. PET water bottles were collected by the authors, cut into smaller pieces, thoroughly washed with soap and water, and then dried with acetone. The PET flakes were further dried in a vacuum oven at 60 °C before use.

2.2. Characterization

^{1}H-NMR spectra were obtained using 500 MHz Bruker Avance instruments (Madison, WI, USA). Thermal transitions were measured *via* differential scanning calorimetry (DSC) using a TA Instruments Discovery DSC-250 instrument with an autosampler capability equipped with a refrigerating cooling system RCS40 (New Castle, DE), from −40 °C to 250 °C with a scan rate of 10 °C min^{-1} under N_2 for three heating–cooling cycles.

Thermogravimetric analysis (TGA) was conducted to determine the thermal stability of the neat PA-ionenes using a TGA7 (PerkinElmer, Inc.) with an alumina sample holder. A Pyris program was used for data handling and analysis. All TGA measurements were performed by heating the samples (~7–28 mg) from ambient temperature to at least 800 °C, at a heating rate of 10 °C min^{-1} under ultrahigh-pure N_2 (UHP300, Airgas) atmosphere at a flow rate of 10 cm^3 min^{-1}.

FTIR spectra were collected using a PerkinElmer Spectrum 2 with an ATR-FTIR attachment (Waltham, MA). Scanning electron microscopy (SEM) images were produced on a Thermo Fisher Apreo SEM (Waltham, MA) or a JEOL 7000 FE Scanning Electron Microscope (Akishima, Tokyo, Japan).

The wide-angle X-ray diffraction (WAXD) patterns of the materials were recorded using a Bruker D8 Discover diffractometer (Billerica, MA) having a 2θ range of 5–60° with a CoKαX ray radiation ($\lambda = 0.17886$ nm) source operated at 40 kV and 35 mA with a scanned step size of 4° min^{-1}. The solid samples were tightly filled in the sample holder and run for 900 s. The *d*-spacing values were calculated using Bragg's law ($d = \lambda/(2\sin\theta)$).

FDM 3D printing was performed using a 3D Bioplotter (Desktop Metal, Germany) equipped with dual print heads capable of operating at temperatures up to 250 °C. The extrusion pressure ranged from 5–7 bar and was supplied by an air compressor.

Tensile testing was performed using a compact, table-top, electromechanical-driven, single-column load-frame universal testing machine (Test Resources Inc, Shakopee, MN, USA), which is equipped with a 1.1 kN load cell capacity. This machine operates over a speed range of 0.01 to 30 in min^{-1},

controlled by Newton software. The mechanical properties of the specimens were evaluated in a controlled environment maintained at 21 ± 2 °C, following ASTM D 638 standards.

2.3. Synthetic procedures

2.3.1 Synthesis of monomeric precursors. PET flakes (6–7 mm in size) (15 g, 78 mmol of repeat units) and MEA (100 g, 1641 mmol) were introduced into a 250 ml heavy-walled round-bottom flask equipped with an egg-shaped magnetic stirrer and heated to 180 °C. After 1.5 h, the PET particles had fully dissolved, and the reaction was allowed to continue for an additional 3 h to ensure thorough mixing. The mixture was then cooled to ambient temperature, during which a slow crystallization of the product was observed. The next day, the mixture was placed in a refrigerator (3 °C) for 24 h to accelerate the crystallization. Acetone was then added to dissolve the recrystallized solid, followed by the addition of dichloromethane (DCM) to induce precipitation. The resulting mixture was filtered and washed with 3 × 200 mL DCM. The white solid obtained, identified as bis(2-hydroxyethyl) terephthalamide ("PET-MEA"), was then dried under vacuum overnight at 60 °C (16.5 g, 65 mmol, 83%). PET-3A1P and PET-DGA were obtained *via* a similar procedure using 3A1P and DGA, respectively, while precipitation of the PET-DGA compound was achieved using EtOAc. More details are included in Table 1. ^{1}H NMR characterizations of these molecules are provided in the ESI (Fig. S1(a), S2(a) and S3(a)†).
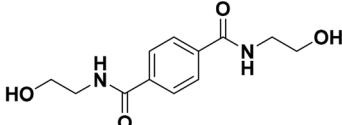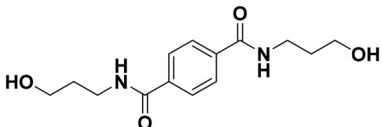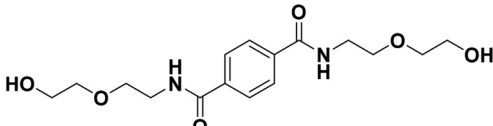
2.3.2 Chlorination of terephthalamide-diols. PET-MEA (16 g, 63 mmol) was placed in a round-bottom flask along with an excess of $SOCl_2$ (45 g, 380 mmol) and pyridine (5 g, 63 mmol). The mixture was heated at reflux overnight (~16 h) to ensure a complete reaction. Following the reflux, the excess $SOCl_2$ was recovered by vacuum distillation. The reaction mixture was then poured into a large excess of deionized (DI)-H_2O, precipitating the desired compound, bis(2-chloroethyl) terephthalamide (PET-MEA-Cl). The precipitate was collected and dried under vacuum at 45 °C overnight (14 g, 48 mmol,

76%). PET-3A1P-Cl (16.5 g, 52 mmol, 73%) and PET-DGA-Cl (18 g, 47 mmol, 80%) were obtained in a similar manner. The complete conversion of –OH to –Cl groups was verified by ^{1}H NMR analysis (Fig. S1 (b), S2(b) and S3(b)†).

2.3.3 Synthesis of bisimidazole monomers. Synthesis of the bisimidazole monomers was performed following previously published procedures.[30] Imidazole (30.0 g, 440 mmol) was gradually added to a mixture of THF (700 mL) and NaH (60 wt% dispersion in mineral oil, 24 g, 969 mmol) in a three-neck round-bottom flask equipped with a reflux condenser. The reaction mixture was heated at 40 °C for 1 h. Subsequently, DBH (49 g, 200 mmol) was introduced *via* syringe, and the reaction was allowed to proceed overnight at reflux (~68 °C) under Ar atmosphere. Upon completion, the solids were filtered and washed with THF. The filtrate was concentrated by rotary evaporation, extracted into MeOH, and washed with hexanes to remove the mineral oil. The methanol layer was then evaporated, and the resulting solid was purified by dissolving in DCM and passing through basic alumina. After evaporation, the DCM layer yielded an off-white bisimidazole solid as 1,1′-(1,6-hexanediyl) bisimidazole (C_6-im$_2$) (40.5 g, 185.5 mmol, 93%). A similar protocol was applied to obtain 1,1′-(1,6-hexanediyl)-2-methylbisimidazole (C_6-mim$_2$) from 2-methylimidazole, yielding 85% (42 g, 170 mmol). ^{1}H NMR analysis confirms the purity of products in agreement with previously published data (Fig. S4a and b†).

2.3.4 PA-ionene synthesis. Stoichiometric quantities of dichloro compound (PET-MEA-Cl, 8.00 g, 27.7 mmol), C_6-im$_2$ (6.04 g, 27.7 mmol), and a small quantity of catalyst, potassium iodide (KI, 0.045 g, 0.27 mmol) were introduced into a 250 mL heavy-walled round-bottom flask (Ace Glass) equipped with a magnetic stir bar. DMAc was used as a solvent for the step-growth polymerization, which occurs *via* the Menshutkin reaction, conducted at 140–150 °C for 16 h. During this time, a gel was observed to collect along the vessel wall, indicating the formation of a high molecular weight polymer. Upon cooling

Table 1 TAm-diol products from the depolymerization of PET by alkanolamines

Identifier	TAm-diol	Yield (%)
PET-MEA		83
PET-3A1P		84
PET-DGA		88

to room temperature, the solvent layer was decanted, and DI water was added to the flask. The mixture was gently heated to dissolve the gel. Concurrently, 3 eq. of LiTf$_2$N salt were dissolved in DI water in an Erlenmeyer flask. The ionene-containing aqueous solution was then poured into the vigorously stirred aqueous LiTf$_2$N solution, facilitating a rapid anion exchange from Cl$^-$ to bistriflimide (Tf$_2$N$^-$), resulting in the precipitation of the hydrophobic PA-ionene. The PA-ionenes were subsequently dried in an oven at 100 °C for 72 h before characterization and used in 3D printing. Using the same procedure, the other PA-ionenes were obtained with good yield (Table 2, S1†). ^{1}H NMR spectra are provided in Fig. S5–S10.† The PA-ionenes structures, names, labels, and yields are shown in Table 2.

Table 2 Identifier, structures, and recovered yields of the prepared PA-ionenes

Identifier	PA-ionene structure	MW R.U. (Da)[a] total/backbone only	Yield (%)
MEA-im		995/434.46 (43.7 wt%)	76.0
MEA-2mim		1023/463 (45.2 wt%)	54.0
3A1P-im		1025/465 (45.3 wt%)	70.0
3A1P-2mim		1053/493 (46.8 wt%)	83.0
DGA-im		1085/525 (48.4 wt%)	73.0
DGA-2mim		1113/553 (49.7 wt%)	78.0

[a] All PA-ionenes shown have two Tf$_2$N$^-$ anions whose combined mass is 560 Da.

3. Results and discussion

The structural identification of all PA-ionenes was confirmed through ATR-FTIR with the corresponding spectra provided in the ESI. Fig. S11† compares the FTIR spectra of monomers and PA-ionene starting from TAm-diols to form ionene *via* step-growth polymerization. Distinguishably, the broad-spectrum ranges around 3500–3000 cm^{-1} for symmetric νOH and νN–H vibrations in the MEA-im PA compound became thinner in the chlorinated amide and ionene compounds. It is worth underlining that, due to the introduction of charge and hydrophobic –CF$_3$ group from Tf$_2$N$^-$ anion, the intensity to the previously assigned band is greatly reduced for the C(2)–H and C(2)–CH$_3$ imidazolium cations formed as a result of polymerization.

Fig. S12† presents the precise identification of specific bonds between atoms and functional groups present in each ionene. The presence of functionalities associated with 2° amide N–H stretching (3400 cm^{-1}), the corresponding C–N bending (1350 cm^{-1}), and carbonyl group C=O (1655 cm^{-1}) were evident in all spectra. Additionally, aromatic and alkyl C–H stretching vibrations were observed at approximately 3150 cm^{-1} and 2850 cm^{-1}, respectively. In these PA-ionenes, the Tf$_2$N$^-$ anion, comprising almost 50% of the molecular weight of the repeat unit, was distinctly identified by the absorption peaks corresponding to the S–N–S system ($\approx$1055 cm^{-1}), symmetric SO$_2$ stretching ($\approx$1180 cm^{-1}) and the hydrophobic –CF$_3$ group ($\approx$1226 cm^{-1}).

^{1}H NMR spectra were used to quantify ionene formation *via* the Menshutkin reaction. As shown in Fig. S5, S7 and S9,† imidazolium C(2)–H shifts are at the most downfield signal at δ 9.18 or higher ppm, revealing the successful quaternization of imidazole groups. The cationic nature of the imidazolium ring, being highly electronegative, has caused the same magnetic environment in almost all spectra at low field, resulting in the shift of C(4)–H and C(5)–H protons to between δ 7.74 to 7.7 ppm. Aliphatic protons having higher electron density showed up in the upfield region, ranging from δ 4.4 ppm to 1.2 ppm. Utilizing C(2)–CH$_3$ bisimidazole monomers, the C(4)–H and C(5)–H shifts appear at ~7.6 ppm in the absence of the C(2)–H proton, which also confirms polymerization of the monomers (*via* conversion from the neutral imidazole to a cationic imidazolium ring) (Fig. S6, S8 and S10†). Finally, if symmetry across all repeating unit structures was noted, the sole benzene ring protons are clearly present at approximately δ 7.8 to 7.9 ppm in all the PA-ionenes in accordance with the ^{1}H NMR spectra of –Cl or OH-containing monomers (Fig. S13 and S5–S10†). The purity obtained by monitoring ^{1}H NMR of the repeating unit of polymers, we assume that 98–99% conversion of the monomers was achieved due to the absence of any obvious signals associated with unreacted imidazole or halide endgroups, which indicates that high molecular weight PA-ionenes of ~50 kDa were obtained, which is consistent with our prior works.

WAXD patterns were obtained to elucidate the interchain packing of these PA-ionenes (Fig. 2). The absence of sharper narrowed intense peaks and the presence of broadened halos indicate the disruption of the PET crystalline phase during synthetic modification, confirming mostly amorphous nature of PA-ionenes.[31,32] However, a distinction was noted between the top four ionenes, which exhibited a single broad halo, and the bottom two (*e.g.*, DGA ionenes), which displayed multiple smaller halos instead of a pronounced peak. This variation may be explained by microcrystallization facilitated by H-bonding arising from intramolecular interactions within the ionene macromolecules, a phenomenon previously reported by Murthy for certain aliphatic PAs (*i.e.*, Nylons).[33] The XRD patterns shown for orderly-arranged nylon PA-6 are quite similar to that we observed for the top 4 ionenes. A recent study by Ma *et al.* on semicrystalline PAs demonstrated that H-bonding does not directly induce crystallinity but plays a crucial role in facilitating the development and stabilization of small crystalline phases under thermal and mechanical conditions.[34] There might also be shear-induced formation of crystal nuclei while processing PAs due to their SH property; they experience stretching and relaxing back to original shape leading to the alignment of chains in a small-scale order in these PA-ionenes.[7,35] The surface morphology analyzed by SEM (Fig. S16†) also reveals the presence of small crystalline domains in these PA-ionenes. In addition, the behavior exhibited by DGA ionenes was explained by Zhou *et al.*, where they found introducing ether (–O–) linkages into an imidazolium-based ionic structure caused the lowering in viscosity and prohibition of crystallization in the final material.[36]

It was also noted, regardless of the imidazolium cation (*i.e.*, C(2)–H or C(2)–CH$_3$), the top 4 PA-ionenes exhibited similar broad halos, with the center of the distribution or primary halo positioned between $2\theta = 19°–24°$ and a secondary, lower-intensity halo extending across $2\theta = 30°–54°$ (Table 3). Bragg's law was applied to determine the d-spacing values with Diffrac.EVA software. These d-spacing values, which fall within the narrow range of 3.72–4.9 Å for the central halo, are consistent with those observed in previously synthesized imidazolium-based PA and PI-ionenes in recent years from our group, suggesting minimal influence from the more linear aliphatic backbone structure in XRD.[19,37,38] The diffraction profiles typically reflect on the packing density and intermolecular interactions in the amorphous or semi-crystalline phase. It is challenging, however, to predict diffraction patterns for polymers with similar archetypes, as slight variations in the position and type of linkers can lead to minor differences in intersegmental distances.

Interestingly, the MEA and 3A1P PA-ionenes with imidazolium C(2)–CH$_3$ substituents exhibited slightly higher d-spacing values, suggesting weaker associations between chains, consistent with observations in the previously studied PI ionenes containing analogous C(2)–CH$_3$ counterparts.[22] This behavior is likely attributable to the presence of the pendant –CH$_3$ group at the C(2) position, which introduces steric hindrance, reducing anion mobility and slightly affecting H-bonding interactions.[39,40] Consequently, this may reduce entanglements and increase the average interchain distance. These
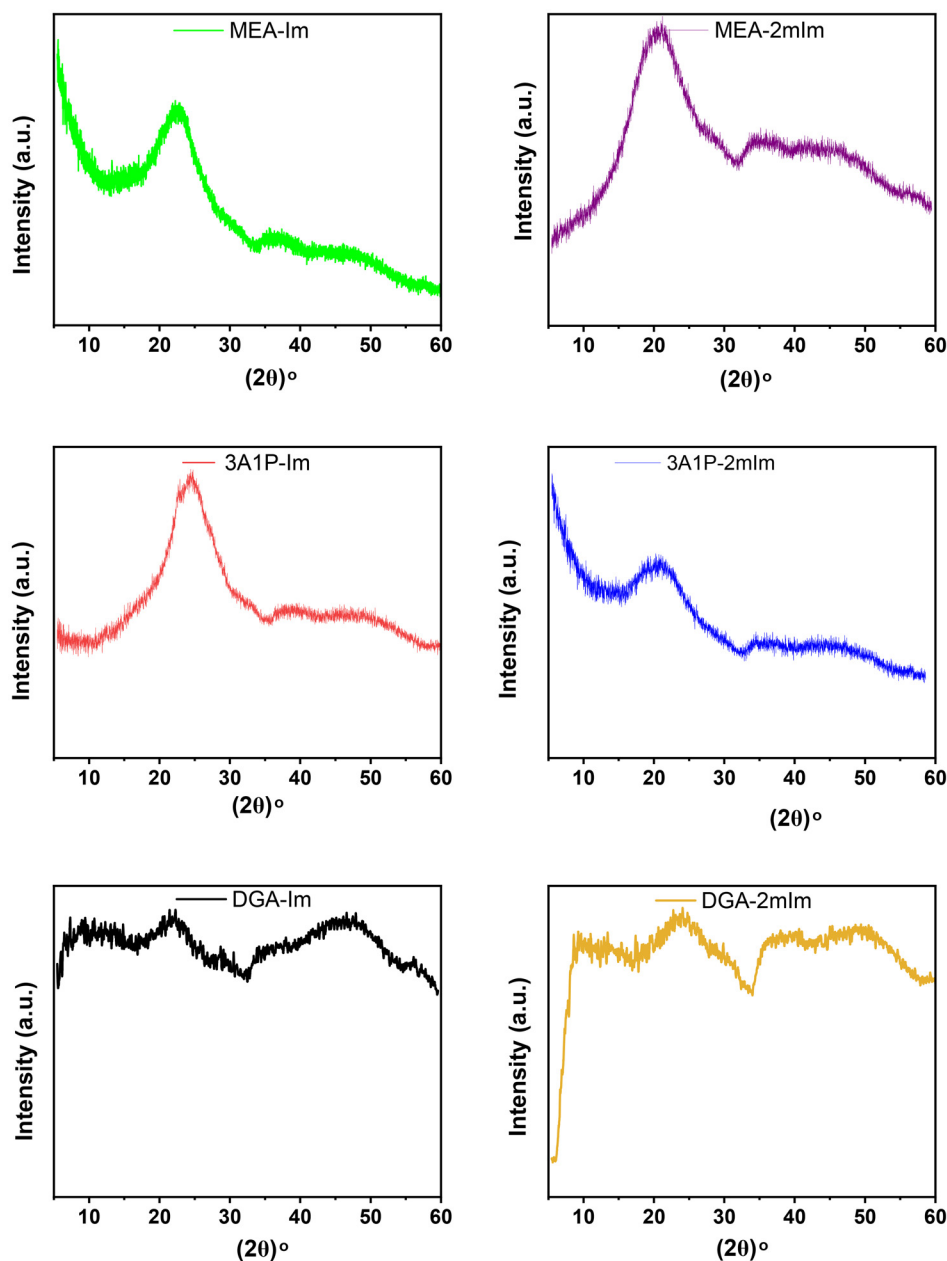
© 2025 The Author(s). Published by the Royal Society of Chemistry

RSC Appl. Polym., 2025, **3**, 686–700 | **693**

Fig. 2 XRD profiles for six separate PA-ionene materials (left = C_6-im$_2$, right = C_6-mim$_2$). Top: MEA. Middle: 3A1P. Bottom: DGA.

Table 3 Glass transition temperature (T_g), melting point (T_m), and d-spacing for each PA-ionene synthesized

Ionene	T_g (°C)	T_m (°C)	d-Spacing (Å)
MEA-im	6.11	220.3	4.0
MEA-2mim	26.39	222.5	4.7
3A1P-im	10.1	159.5	4.3
3A1P-2mim	11.74	221.4	4.9
DGA-im	−7.3	209.9	4.1
DGA-2mim	1.34	207.0	3.9

materials also demonstrated increased stiffness during physical handling, as evidenced by the properties of fibers extruded using the 3D Bioplotter, compared to their C(2)–H-imidazolium counterparts. For the DGA PA-ionenes, the d-spacing values were similar to each other as well as MEA-Im, where the presence of H-bonding from C(2)–H with the surrounding anion played a role in regularity and ordering between chains. Also, the competitive interactions between ether O atoms and Tf$_2$N$^-$ anions for imidazolium cations may be a contributing factor to the multiple halo XRD profile of DGA-im and DGA-2mim PA-ionenes.[36,41,42]

As thermal properties are vital in determining the proper operating parameters for FDM 3D printing, TGA and DSC characterization provide key information regarding stability, phase transitions, and overall thermal behavior. TGA was conducted under an N$_2$ atmosphere from 25 °C to 800 °C to assess

the thermal stability of PA-ionenes (Fig. S14†). Previous studies have revealed that imidazolium ionenes exhibit comparatively higher degradation temperatures (>250 °C) than other N-based cationic moieties (*e.g.*, ammonium, pyridinium) which have stabilities ≤200 °C.[17,43] Furthermore, research on the impact of counterions discovered that larger organic anions (*i.e.*, Tf_2N^- and triflate (OTf^-)) provide greater thermal resistance at elevated temperatures compared to smaller inorganic anions (*i.e.*, Cl^-, PF_6^-, BF_4^-).[44] Consequently, the anion exchange from Cl^- to Tf_2N^- significantly enhanced the thermal stability of each ionene, with an onset degradation temperature (T_d) approaching 350 to 380 °C. Beyond 380 °C, a gradual decrease in mass was observed, followed by an inflection point near 68% mass loss, which is likely attributed to the initial degradation of the Tf_2N^- anion, as it constitutes ~50 wt% of the overall polymer mass (Table 2). The second stage of degradation, beginning around 450 °C and marked by a distinct curvature, likely corresponds to the decomposition of the primary PA-ionene backbone and the residual char.

Compared to our work with PA-ionenes with adipamide linkages, PA-ionenes with TAm backbone are more thermally stable (292 *vs.* 350 °C).[45] The observed mass loss pattern aligns with that of other PA-ionenes synthesized from *p*-xylene motifs or ionenes with increased aromaticity, suggesting that the alkyl spacer may have a limited influence on the breakdown or disentanglement of chain–chain packing or the degradation of the polymer backbone underscoring their robustness processing at elevated temperatures.[37]

T_g and T_m values for the PA-ionenes were determined using DSC (Fig. 3b and S15†) and meticulously examined over three

cycles at a scan rate of 10 °C min^{-1}, which is documented in Table 3. Although previously synthesized ionenes from our lab were identified as amorphous with only a T_g, these PA-ionenes may contain microcrystalline regions, as illustrated by the XRD and SEM profiles (Fig. S16†), which reveal small endothermic peaks (T_m) in the DSC thermograms. The single T_g value for all the ionene suggests the homogeneity of the PA backbone with well-integrated cation–anion pairs. However, the observed broadening and reduction in T_g for specific PA-ionenes (*i.e.*, DGA-im, DGA-2mim) can be attributed to the same factors highlighted in the XRD profiles in Fig. 2. This finding aligns with the observation reported by Meyer *et al.*, where increased chain alignment was driven by the longer distance of the anion from the main-chain cation, affecting the compactness of material and thereby lowering the T_g for ether-linked PA materials.[43,46] Nonetheless, as exhibited in Fig. 3a, these materials present SH properties, as demonstrated with the DGA-2mim compound. A hole created at the center was almost repaired within 48 h without external stimuli, leaving no visible damage on the thick film.

Additionally, individual fibers were successfully extruded to form simple geometries from ether-linked ionic compounds, such as a solid disc, at temperatures between 70 to 80 °C using a 3D Bioplotter (Fig. S16†). At the same time, the DGA-im ionene was found to be tacky, resulting in low-quality 3D-printed objects. On the contrary, higher T_g values were noticeable in the PA-ionenes with imidazolium C(2)–CH_3 groups (*i.e.*, 3A1P-2mim and MEA-2mim), which is comparable to properties found in ILs having C(2)–CH_3 in the imidazolium ring with tangible increased rigidity.(39) Notably, unlike other PAs,
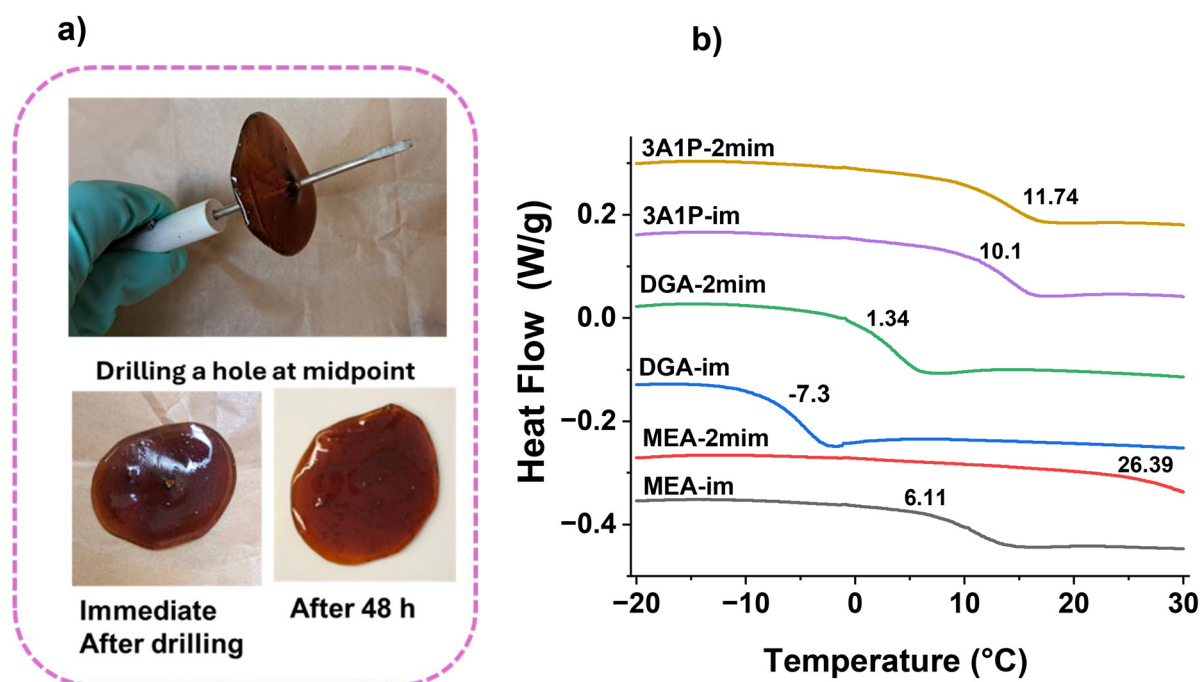

Fig. 3 (a) Self-healing of a thick film prepared from PET-derived PA ionene, DGA-2mim. (b) DSC thermograms for all six PA ionenes.

double melting peaks were observed for MEA-2mim ionene. This could indicate the formation of a small crystalline region at low temperature (206.52 °C) and the higher peak (222.53 °C) is responsible for the dominant ionene backbone as explained by Tan *et al.*,[47] which correspond to considering T_m as 222.53 °C for MEA-2mim.

Fig. 4 and 5 depict the printed parts of PA-ionenes sourced from waste PET using an Envsiontec-3D Bioplotter (Starter Series) using the high-temperature extruder. The objective was to assess the printability of various PA-ionenes based on their molecular compositions and obtain specimens for measuring mechanical (*i.e.*, tensile) tests. The DSC and TGA analyses performed aided in determining process parameters crucial for FDM printing. Initially, small discs (~2 cm diameter, 1.2 mm thick) were printed as test samples before progressing into the larger bars for tensile testing. Interestingly, despite consisting of common functional groups within the macromolecule structures, the melt extrusion temperature (T_{mx}) and flow rate significantly varied for different materials (Table S2†). T_{mx} was found to be lower than their endothermic melting peak (T_m) observed in the DSC thermogram, except for the 3A1P-im PA-ionene exhibiting elevated T_{mx} rather than T_m. Both the 3A1P-im and 3A1P-2mim PA-ionenes were able to print delicate designs showing minimal warping and shrinkage post-extrusion and producing surfaces with smooth finishes (Fig. 4b), while 3A1P-2mim was more accurate in holding strength of the fiber, delivering a smooth printed texture, and optical clarity (Fig. 5). Fig. S18† displays four similar puzzle blocks printed from the 3A1P-im ionene. When these were united, they demonstrated intrinsic SH at the interfaces between the pieces.

Similarly, the same material shows gradual SH when cut at the midpoint, as observed *via* SEM (Fig. S19†). The SH behaviors are likely the result of H-bonding of the delocalized Tf_2N^- anion bridging with imidazolium cations. It is worth noting that the Tf_2N^- anions comprise ~50% by mass of the overall material (Table 2), so their contribution to PA-ionene properties is significant. Additionally, conventional amide H-bonding is expected to contribute to the SH characteristics in these ionenes.

Additionally, the C(2)–CH$_3$ group appears to impart rigidity to the 3A1P-2mim structure while also promoting good adhesion within and between layers, as seen in Fig. 5. The linear infill orientation of this material was also distinctly visible in the SEM images of both the disc and rectangular slab. To better understand the morphology of the self-healed part, SEM and optical microscopic images were captured and presented in Fig. S20 and 21.† Imaging of fibers also highlights the high-quality of these PA-ionene compounds for extrusion (Fig. S22†). The DGA-im, DGA-2mim, and MEA-im PA-ionenes could be extruded at lower temperatures (70 to 80 °C); however, these materials exhibit deformation within 2–3 d of printing as well as tackiness. A significant change in stiffness was observed for the PA-ionenes with imidazolium C(2)–CH$_3$ substitution, making the backbone more robust and affecting their flow properties.[48] This phenomenon caused a positive alteration in DGA-2mim and 3A1P-2mim PA-ionenes, whereas MEA-2mim could not be extruded even at 180 °C. The phenomenon is most likely due to a higher melt viscosity, which prevents extrusion from the 0.4 mm nozzle with the maximum available air pressure (7 bar).

To improve the extrusion properties of the MEA-2mim ionene, [C$_4$mim] [Tf$_2$N] IL was added at 28% by weight (*i.e.*, 1 eq. IL added per ionene repeat unit), which caused the mixture to swell. Complete mixing was achieved by dissolving the PA-ionene + IL in 8 mL DMAc solvent and casting it onto a
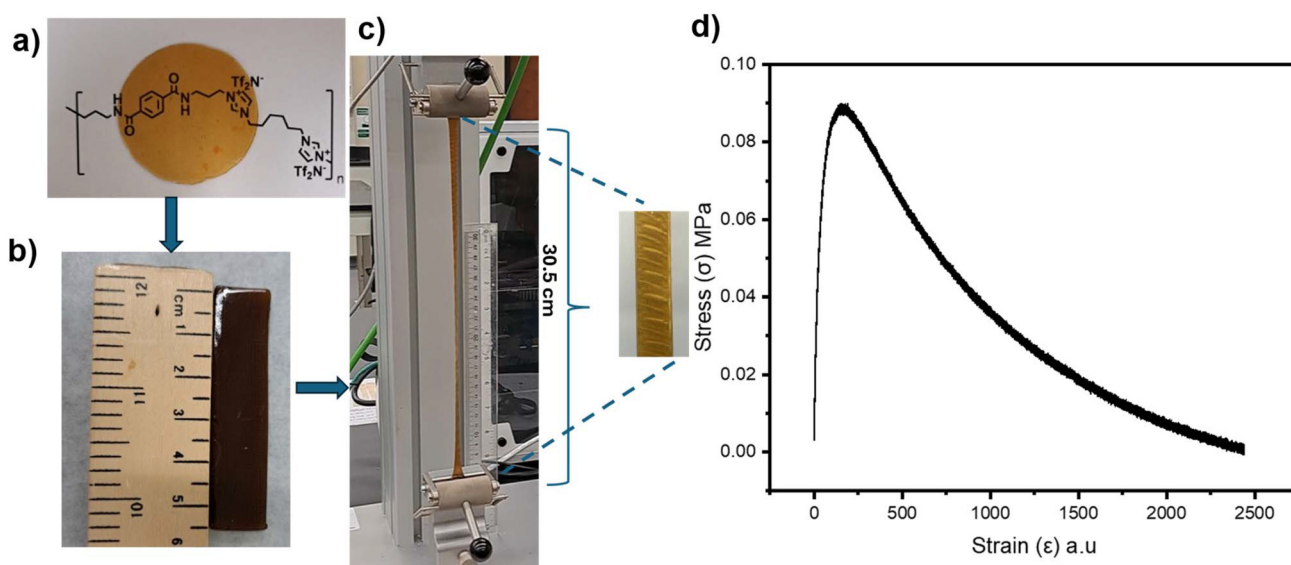

Fig. 4 (a) A thin film prepared from 3A1P-im PA-ionene at RT. (b) 3D-printed slab specimen made *via* FDM at 170 °C (10 layers, 3.2 mm total thickness). (c) Tensile testing of the slab showing high elongation at break. (d) Stress−strain plot of the resultant stress.
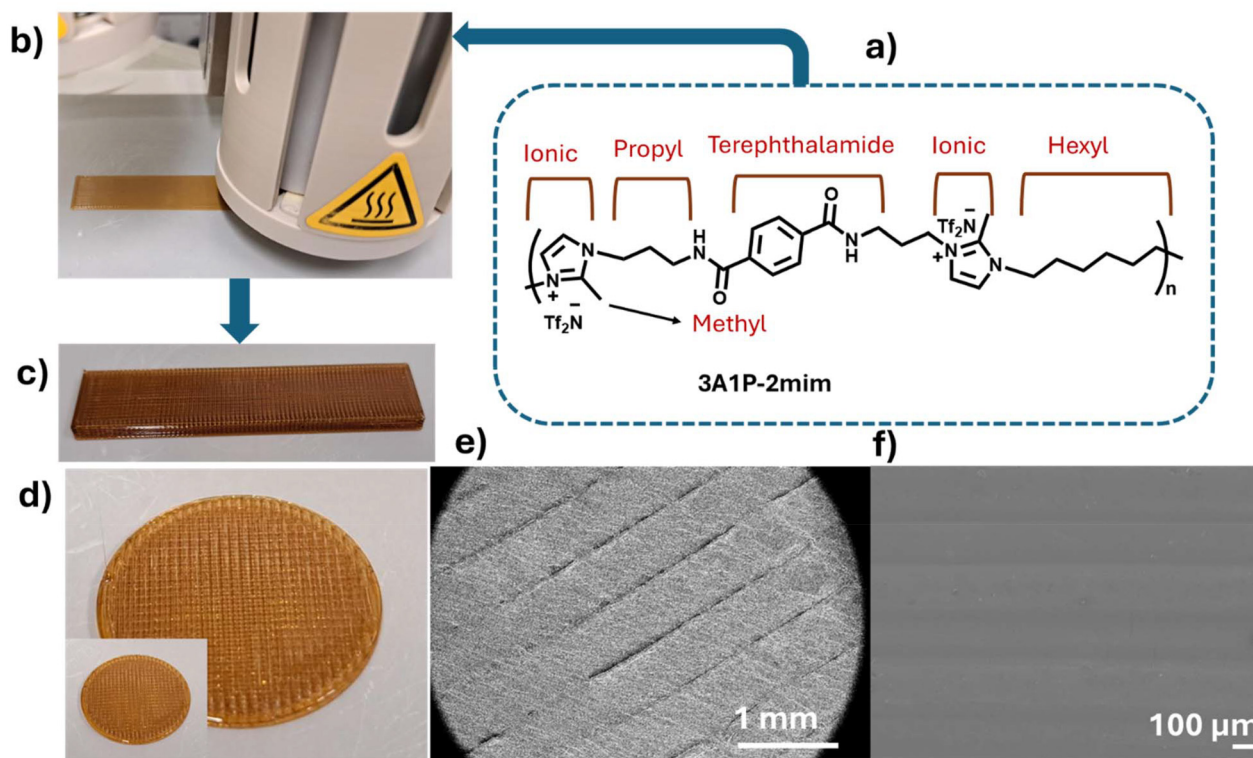
Fig. 5 (a) Repeat unit structure and segments of 3A1P-2mim PA-ionene contributing intramolecular interaction. (b) 3D printing of first two layers of a slab (~0.66 mm thickness at this point). (c) Completed slab (9 layers, ~2.88 mm thickness). (d) 3D printed disc (5 layers, 1.2 mm thickness. (e) SEM infill pattern orientation for 3D printed slabs and discs. (f) Stretching was observed in the SEM image of the slab after tensile testing.

PTFE plate. The solvent was allowed to evaporate in an oven at 120 °C over 3 d. The resulting PA-ionene + IL composite could be extruded at 75 °C, exhibiting increased flexibility and tackiness, although the print resolution appeared to diminish (Fig. S23†).

Ultimate tensile strength (UTS), elongation at break, and tensile toughness were assessed using a UTM instrument with a 0.0254 m min⁻¹ pulling rate. The entire stress–strain curve for all PA-ionenes synthesized is presented in Fig. S24.† The experiment indicated that the precise elongation at break could not be accurately measured, as the samples' elasticity exceeded the instrument's travel distance (30.5 cm), resulting in unexpectedly low tensile strength for the 3D-printed slabs, accompanied by a dramatic rise in flexibility. This lower strength implies an increased aliphatic nature of the main chain backbone, which could likely be improved with a shorter alkyl spacer (C_2 or C_4 instead of C_6) between the imidazolium cations. However, the stress–strain behavior is consistent with thermoplastics and elastomers, as reviewed by Herzberger and co-workers, where elastomers characteristically exhibit substantial, reversible strains while maintaining minimal stress levels.[25] The representative stress–strain profiles for each ionene are shown in Fig. 6, indicating that PA-ionenes with C(2)–CH₃ cations are comparatively stiffer than those with analogous C(2)–H imidazolium cations, where they experienced more elongation. This finding is quite similar to those

obtained by imidazolium based ILs. It was found that imidazolium cations with $C(2)$–CH_3 groups enhance the rotational barrier between the cation and anion while bringing closer contact with the backbone, which is affected by increasing melting point and viscosity in the methylated ILs, also observed by the synthesized ionenes in this work. Contrarily, $C(2)$–H-based ionenes have the free rotational space for anion with enhanced H-bonding, resulting in flexible movement.[39] This flexibility was coupled by the extended order of linear organic chain segments of hexyl spacer linking to the cationic centers of the TA backbone, providing more space for rotation of the ion-pair complex in the polymer molecules, resulting in moderate strength. Remarkably, these ionenes could be manually stretched up to 4 m without rupture. Alternatively, the melt-casted MEA-2mim-ionene exhibited significant stiffness, showing no elongation and UTS of 1.25 MPa.

Among the rest of the flexible materials, 3A1P-2mim possessed a balance of good strength, having elongation at 3600%, UTS of 0.65 MPa and a toughness of 4432 MJ m⁻³, which seems to possess the best combination of properties observed from dimensional accuracy and longer retention of infill orientation of 3D printed objects across all the PA-ionenes studied here. The self-healed rectangular bar of this ionene showed 3100% elongation with a loss of only 13.5% (Fig. S25†). It also demonstrated shape memory (SM) behavior (Fig. S26†), an action not observed in other PA-ionenes. The
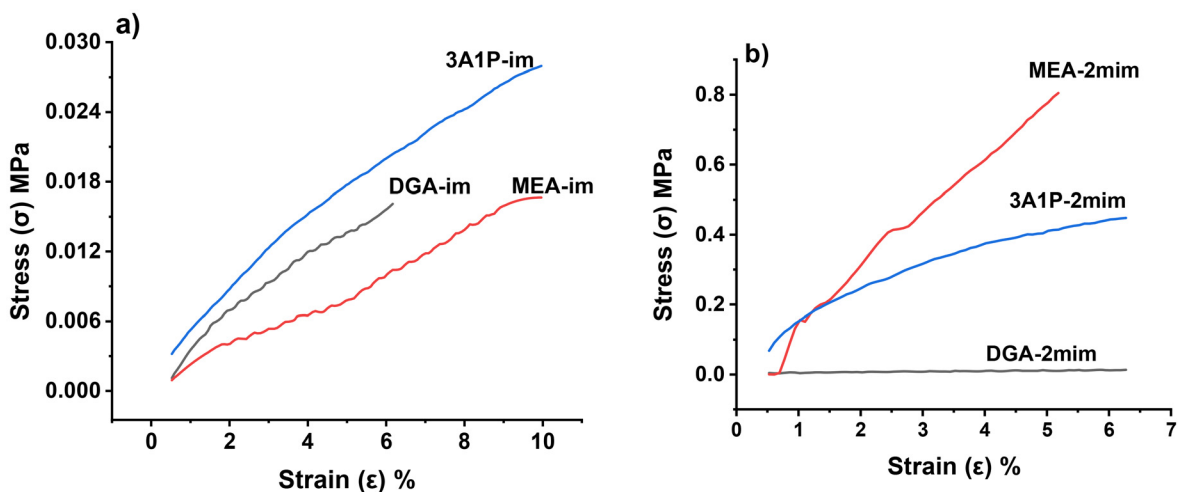
© 2025 The Author(s). Published by the Royal Society of Chemistry

RSC Appl. Polym., 2025, **3**, 686–700 | **697**

Fig. 6 Representative modulus of elasticity (ε) from stress−strain curves for PA-ionenes with (a) C(2)−H imidazolium cations and (b) C(2)−CH$_3$ imidazolium cations.

stretched slab from the same material recovered 70% of its initial length within 10–15 min after releasing the load followed by tensile testing (Fig. S27 and Video S1†). Interestingly, in terms of mechanical strength, an anomaly was observed with the PA-ionene synthesized from *p*-xylene motif [TC-API(*p*)-Xy][Tf$_2$N], where it had UTS of 8 MPa and 454% elongation, showing good strength possibly due to the additional aromatic character associated with the *p*-xylyl linkage.[26] This latter material was used to assemble a dodecahedron from essentially 2D parts that underwent SH and fused into a single 3D object.

Thus, evaluating the mechanical performance of literature-reviewed ionene and this work, our study shows that PA-ionenes using monomers derived from PET and commodity alkanolamines have obvious effects on thermal and mechanical properties and the associated processability for extrusion and 3D printing. This understanding will aid in tailoring structures with the choice of monomers synthesized from waste PET (or *via* conventional reactions with TC), depending on the desired properties. However, we also note that the role of the bisimidazole comonomer is important and that there are many possibilities to increase PA-ionene strength with shorter and/or different spacers between the imidazolium cations. Furthermore, the addition of "free" ILs can also have a significant impact on improving processability and properties if the PA-ionene is too stiff to be extruded *via* FDM 3D printing. Finally, the contribution of 2° (N–H) *vs.* 3° (N–CH$_3$) amides is another aspect of PA-ionenes that will be examined in future works.

4. Conclusions

In this work, we employed well-known but perhaps underutilized methods that use commodity alkanolamines (MEA, 3A1P, DGA) for the depolymerization of post-consumer PET to obtain

TAm-diols which were then converted to the corresponding α,ω-dichloro compounds. These molecules were then polymerized with bisimidazole compounds *via* the Menshutkin reaction, followed by anion exchange to obtain six different PA-ionenes. The PA-ionenes were thoroughly characterized and demonstrated good thermal and mechanical properties, as well as the ability to be 3D printed *via* FDM techniques. As in our prior works, these PA-ionenes were also intrinsically self-healing. Furthermore, it was shown that for a PA-ionene which could not be extruded within the limitations of the 3D printer, the addition of "free" IL into the PA-ionene was able to improve processability such that the PA-ionene + IL composite could be extruded and printed. While this work only studied 6 new PA-ionenes, there are many more backbone-anion combinations that can be synthesized and analyzed to further understand the structure–property relationships and SH mechanisms. Likewise, the ability to obtain at least one of the monomers from commodity alkanolamines and waste PET may represent a major step forward in making ionenes much more accessible for 3D printing and many other applications.

Data availability

The data supporting this article have been included in the ESI.†

Conflicts of interest

There are no conflicts to declare.

Acknowledgements

References

1 R. Geyer, J. R. Jambeck and K. L. Law, Production, use, and fate of all plastics ever made, *Sci. Adv.*, 2017, **3**(7), e1700782.

2 Plastics ocean 2022 [Available from: **https://plasticoceans. org/the-facts/**].

3 J. Di, B. K. Reck, A. Miatto and T. E. Graedel, United States plastics: Large flows, short lifetimes, and negligible recycling, *Resour., Conserv. Recycl.*, 2021, **167**, 105440.

4 R. L. Smith, S. Takkellapati and R. C. Riegerix, Recycling of plastics in the United States: plastic material flows and polyethylene terephthalate (PET) recycling processes, *ACS Sustainable Chem. Eng.*, 2022, **10**(6), 2084–2096.

5 E. Barnard, J. J. R. Arias and W. Thielemans, Chemolytic depolymerisation of PET: a review, *Green Chem.*, 2021, **23**(11), 3765–3789.

6 R. Blanchard and T. H. Mekonnen, Valorization of plastic waste via chemical activation and carbonization into activated carbon for functional material applications, *RSC Appl. Polym.*, 2024, **2**(4), 557–582.

7 Plastics – the fast Facts 2023 2023 [Available from: **https:// plasticseurope.org/knowledge-hub/plastics-the-fast-facts-2023/**].

8 Polyethylene Terephthalate (PET) Market Size, Share & Industry Analysis Source: **https://www.fortunebusinessin-sights.com/industry-reports/polyethylene-terephthalate-pet-market-101743** September 09, 2024.

9 M. D. de Dios Caputto, R. Navarro, J. L. Valentín and Á. Marcos-Fernández, Chemical upcycling of poly (ethylene terephthalate) waste: Moving to a circular model, *J. Polym. Sci.*, 2022, **60**(24), 3269–3283.

10 M. R. Bepari, L. R. Sullivan, K. E. O'Harra, G. D. Barbosa, C. H. Turner and J. E. Bara, Depolymerizing Polyethylene Terephthalate (PET) via "Imidazolysis" for Obtaining a Diverse Array of Intermediates from Plastic Waste, *ACS Appl. Polym. Mater.*, 2024, **6**(13), 7886–7896.

11 F. Barzagli, F. Mani and M. Peruzzini, A comparative study of the CO2 absorption in some solvent-free alkanolamines and in aqueous monoethanolamine (MEA), *Environ. Sci. Technol.*, 2016, **50**(13), 7239–7246.

12 J. E. Bara, What chemicals will we need to capture CO2?, *Greenhouse Gases: Sci. Technol.*, 2012, **2**(3), 162–171.

13 J. Demarteau, I. Olazabal, C. Jehanno and H. Sardon, Aminolytic upcycling of poly (ethylene terephthalate) wastes using a thermally-stable organocatalyst, *Polym. Chem.*, 2020, **11**(30), 4875–4882.

14 E. Bäckström, K. Odelius and M. Hakkarainen, Ultrafast microwave assisted recycling of PET to a family of functional precursors and materials, *Eur. Polym. J.*, 2021, **151**, 110441.

15 B. Li, P.-F. Cao, T. Saito and A. P. Sokolov, Intrinsically self-healing polymers: from mechanistic insight to current challenges, *Chem. Rev.*, 2022, **123**(2), 701–735.

16 K. E. O'Harra and J. E. Bara, Toward controlled functional sequencing and hierarchical structuring in imidazolium ionenes, *Polym. Int.*, 2021, **70**(7), 944–950.

17 J. E. Bara and K. E. O'Harra, Recent advances in the design of ionenes: toward convergence with high–performance polymers, *Macromol. Chem. Phys.*, 2019, **220**(13), 1900078.

18 K. O'Harra, I. Kammakakam, P. Shinde, C. Giri, Y. Tuan, E. M. Jackson, *et al.*, Poly (ether ether ketone) Ionenes: Ultrahigh-Performance Polymers Meet Ionic Liquids, *ACS Appl. Polym. Mater.*, 2022, **4**(11), 8365–8376.

19 K. E. O'Harra, D. M. Noll, I. Kammakakam, E. M. DeVriese, G. Solis, E. M. Jackson, *et al.*, Designing Imidazolium Poly (amide-amide) and Poly (amide-imide) Ionenes and Their Interactions with Mono-and Tris (imidazolium) Ionic Liquids, *Polymers*, 2020, **12**(6), 1254.

20 J. P. Tan, J. Tan, N. Park, K. Xu, E. D. Chan, C. Yang, *et al.*, Upcycling poly (ethylene terephthalate) refuse to advanced therapeutics for the treatment of nosocomial and mycobacterial infections, *Macromolecules*, 2019, **52**(20), 7878–7885.

21 J. Demarteau, K. E. O'Harra, J. E. Bara and H. Sardon, Valorization of plastic wastes for the synthesis of imidazolium–based self–supported elastomeric ionenes, *ChemSusChem*, 2020, **13**(12), 3122–3126.

22 G. P. Dennis, K. E. O'Harra, X. Liu, E. M. Jackson, C. H. Turner and J. E. Bara, Experimental and computational studies on the effects of C (2) methylation on the properties and gas separation performance of polyimide-ionene membranes, *RSC Appl. Polym.*, 2023, **1**(1), 111–122.

23 W. B. Wright Jr, J. B. Press, P. S. Chan, J. W. Marsico, M. F. Haug, J. Lucas, *et al.*, Thromboxane synthetase inhibitors and antihypertensive agents. 1. N-[(1H-imidazol-1-yl) alkyl] aryl amides and N-[(1H-1, 2, 4-triazol-1-yl) alkyl] aryl amides, *J. Med. Chem.*, 1986, **29**(4), 523–530.

24 H. Nulwala, A. Mirjafari and X. Zhou, Ionic liquids and poly (ionic liquid) s for 3D printing–A focused mini-review, *Eur. Polym. J.*, 2018, **108**, 390–398.

25 J. Herzberger, J. M. Sirrine, C. B. Williams and T. E. Long, Polymer design for 3D printing elastomers: recent advances in structure, properties, and printing, *Prog. Polym. Sci.*, 2019, **97**, 101144.

26 K. O'Harra, N. Sadaba, M. Irigoyen, F. Ruipérez, R. Aguirresarobe, H. Sardon, *et al.*, Nearly perfect 3D structures obtained by assembly of printed parts of polyamide ionene self-healing elastomer, *ACS Appl. Polym. Mater.*, 2020, **2**(11), 4352–4359.

27 A. M. Pekkanen, C. Zawaski, A. T. Stevenson Jr, R. Dickerman, A. R. Whittington, C. B. Williams, *et al.*, Poly (ether ester) ionomers as water-soluble polymers for

© 2025 The Author(s). Published by the Royal Society of Chemistry

RSC Appl. Polym., 2025, **3**, 686–700 | **699**

material extrusion additive manufacturing processes, *ACS Appl. Mater. Interfaces*, 2017, **9**(14), 12324–12331.

28 C. E. Zawaski, C. A. Chatham, E. M. Wilts, T. E. Long and C. B. Williams, Using fillers to tune material properties of an ion-containing semi-crystalline poly (ethylene glycol) for fused filament fabrication additive manufacturing, *Addit. Manuf.*, 2021, **39**, 101844.

29 M. Wang, P. Zhang, M. Shamsi, J. L. Thelen, W. Qian, V. K. Truong, *et al.*, Tough and stretchable ionogels by in situ phase separation, *Nat. Mater.*, 2022, **21**(3), 359–365.

30 J. E. Bara, E. S. Hatakeyama, B. R. Wiesenauer, X. Zeng, R. D. Noble and D. L. Gin, Thermotropic liquid crystal behaviour of gemini imidazolium-based ionic amphiphiles, *Liq. Cryst.*, 2010, **37**(12), 1587–1599.

31 A. Gómez-Valdemoro, N. San-José, F. C. García, J. L. De La Peña, F. Serna and J. M. García, Novel aromatic polyamides with main chain and pendant 1, 2, 4-triazole moieties and their application to the extraction/elimination of mercury cations from aqueous media, *Polym. Chem.*, 2010, **1**(8), 1291–1301.

32 A. Halasa, G. Wathen, W. Hsu, B. Matrana and J. Massie, Relationship between interchain spacing of amorphous polymers and blend miscibility as determined by wide–angle X–ray scattering, *J. Appl. Polym. Sci.*, 1991, **43**(1), 183–190.

33 N. S. Murthy, Hydrogen bonding, mobility, and structural transitions in aliphatic polyamides, *J. Polym. Sci., Part B: Polym. Phys.*, 2006, **44**(13), 1763–1782.

34 R. Ma, L. Zhang, Z. Zhang, C. Huang, H. Huang, W. Cao, *et al.*, Thermal-Induced Structural Evolution of Melt-Stretched PA11: Direct Evidence for the Preservation of Hydrogen-Bonded Sheets Above the Brill Transition Temperature, *Macromolecules*, 2025, **58**(1), 459–472.

35 K. Jariyavidyanont, S. Mallardo, P. Cerruti, M. L. Di Lorenzo, R. Boldt, A. M. Rhoades, *et al.*, Shear-induced crystallization of polyamide 11, *Rheol. Acta*, 2021, **60**, 231–240.

36 Y. Zhou, X. Xu, Z. Wang, S. Gong, H. Chen, Z. Yu, *et al.*, The effect of introducing an ether group into an imidazolium-based ionic liquid in binary mixtures with DMSO, *Phys. Chem. Chem. Phys.*, 2020, **22**(27), 15734–15742.

37 J. E. Bara, K. E. O'Harra, M. M. Durbin, G. P. Dennis, E. M. Jackson, B. Thomas, *et al.*, Synthesis and characterization of ionene-polyamide materials as candidates for new gas separation membranes, *MRS Adv.*, 2018, **3**(52), 3091–3102.

38 I. Kammakakam, K. E. O'Harra, G. P. Dennis, E. M. Jackson and J. E. Bara, Self–healing imidazolium–based ionene–polyamide membranes: an experimental study on physical and gas transport properties, *Polym. Int.*, 2019, **68**(6), 1123–1129.

39 K. Fumino, T. Peppel, M. Geppert-Rybczyńska, D. H. Zaitsau, J. K. Lehmann, S. P. Verevkin, *et al.*, The influence of hydrogen bonding on the physical properties of ionic liquids, *Phys. Chem. Chem. Phys.*, 2011, **13**(31), 14064–14075.

40 S. B. Lehmann, M. Roatsch, M. Schöppke and B. Kirchner, On the physical origin of the cation–anion intermediate bond in ionic liquids Part I. Placing a (weak) hydrogen bond between two charges, *Phys. Chem. Chem. Phys.*, 2010, **12**(27), 7473–7486.

41 G. D. Smith, O. Borodin, L. Y. Li, H. Kim, Q. Liu, J. E. Bara, *et al.*, A comparison of ether- and alkyl-derivatized imidazolium-based room-temperature ionic liquids: a molecular dynamics simulation study, *Phys. Chem. Chem. Phys.*, 2008, **10**(41), 6301–6312.

42 D. H. Zaitsau, A. V. Yermalayeu, S. P. Verevkin, J. E. Bara and A. D. Stanton, Structure–Property Relationships in Ionic Liquids: A Study of the Influence of N(1) Ether and C(2) Methyl Substituents on the Vaporization Enthalpies of Imidazolium-Based Ionic Liquids, *Ind. Eng. Chem. Res.*, 2013, **52**(47), 16615–16621.

43 S. R. Williams and T. E. Long, Recent advances in the synthesis and structure–property relationships of ammonium ionenes, *Prog. Polym. Sci.*, 2009, **34**(8), 762–782.

44 K. E. O'Harra, I. Kammakakam, J. E. Bara and E. M. Jackson, Understanding the effects of backbone chemistry and anion type on the structure and thermal behaviors of imidazolium polyimide–ionenes, *Polym. Int.*, 2019, **68**(9), 1547–1556.

45 K. E. O'Harra, G. M. Timmermann, J. E. Bara and K. M. Miller, Designing Ionic Liquid-Derived Polymer Composites from Poly (Ionic Liquid)–Ionene Semi-interpenetrating Networks, *ACS Appl. Polym. Mater.*, 2021, **3**(4), 1995–2004.

46 W. H. Meyer, R. R. Rietz, D. Schaefer and F. Kremer, Dielectric and electric relaxation in ionene-glasses, *Electrochim. Acta*, 1992, **37**(9), 1491–1494.

47 S. Tan, A. Su, J. Luo and E. Zhou, Crystallization kinetics of poly (ether ether ketone)(PEEK) from its metastable melt, *Polymer*, 1999, **40**(5), 1223–1231.

48 G. S. Bhat, Plastics: materials and processing by A. Brent strong, *Mater. Manuf. Processes*, 1997, **12**(3), 560–562.